Concrete properties at high temperature. Complete characterization of 2 concretes: B40 and B60

J.-C. Mindeguia, Pierre Pimienta, K. Mroz, Hélène Carré, Christian La Borderie

Concrete properties at high temperature – complete characterization of 2 concretes: B40 and B60

Mindeguia J.C.(1), Pimienta P.(2), Mróz K.(3), Carré H.(4), La Borderie C.(4)

1 I2M, University of Bordeaux, France, jean-christophe.mindeguia@u-bordeaux.fr
2 CSTB, Centre Scientifique et Technique du Bâtiment, France, pierre.pimienta@cstb.fr
3 Cracow University of Technology, Cracow, Poland, katarzyna.mroz@pk.edu.pl
4 SIAME, University of Pau and Pays de l'Adour, France, helene.carre@univ-pau.fr and christian.laborderie@univ-pau.fr

Version: 1
Date: 06/05/2024

Concrete properties at high temperature – complete characterization of 2 concretes: B40 and B60

Mindeguia J.C., Pimienta P., Mróz K., Carré H., La Borderie C.

Abstract

The report presents concretes properties at high temperature of 2 concretes B40 and B60.
These properties have been studied extensively in the frame of several research and expertise projects, including thesis projects. The first very detailed characterization at high temperature was performed by Jean Christophe Mindeguia during his PhD thesis.

The report provides the composition of the 2 concretes and their constituents, mass transport properties (porosity, permeability ...), thermal properties, mechanical properties (strength, thermal strain, transient thermal strain, fracture energy…). In addition, the report includes the results from pore pressure and mass loss measurements (PTM) at high temperature.

Finally, a large number of tests have also been carried out on fire exposed intermediate-scale and large-scale specimens made from these 2 concretes. The references of the publications are given at the end of the report.

Table of content

1. INTRODUCTION

The drafting of this report was initiated as part of the work of the RILEM Technical Committee 256-SPF Spalling of concrete due to fire: testing and modelling. More specifically, it was initiated in the task dedicated to modelling work on 2 concretes M100 and B40.

Both concretes have been characterized extensively. The report presents concretes properties at high temperature of 2 concretes B40 and B60.

The reference concrete is an ordinary concrete (B40), which has been used for the construction of a tunnel in France in 2005. The second concrete is fabricated by only varying the W/C ratio (by increasing cement content and reducing water content) and by fixing the aggregates quantity constant.

Their properties have been studied extensively in the frame of several research and expertise projects, including thesis projects. The first very detailed characterization was performed by Jean Christophe Mindeguia during his PhD thesis [1] whose work has given rise to numerous publications [2] to [18].

The report provides the composition of the 2 concretes and their constituents, mass transport properties (porosity, permeability ...), thermal properties, mechanical properties (strength, thermal strain, transient thermal strain, fracture energy…). In addition, the report includes the results from pore pressure and mass loss measurements (PTM) at high temperature.

Finally, a large number of tests have also been carried out on fire exposed intermediate-scale and large-scale specimens made from these 2 concretes. The references of the publications are given at the end of the report.

The characterization of the high performance M100C concrete at high temperature has also been carried out and is summarized in a second report: Concrete properties at high temperature – complete characterization of M100C concrete by Mindeguia J.C., Hager I, Pimienta P., Mróz K. and Carré H..

This report is intended to evolve and be updated as new data are acquired. Readers are invited to contact the authors if they detect any corrections or additions to be made.

2. MATERIALS AND MIXTURES

2.1. Concrete compositions

The B40 and B60 mixtures, as well as the main characteristics of the concretes at 20 °C, are presented in Table 1 [1], [5] and [12]. Compressive strength and modulus of elasticity have been measured at 28 days on Ø 160 mm x h 320 mm cylindrical samples. Tensile strength has been assessed by mean of 28 days splitting test.

For 1 m³ of B40 and B60	Unity	B40	B60
Cement CEM II/A-LL 42.5 R PM-CP2 (C)	kg	350	550
8/12.5 calcareous gravel (*Chalonnes sur Loire*)	kg	330	330
12.5/20 calcareous gravel (*Chalonnes sur Loire*)	kg	720	720
0/2 siliceous sand (*Chazé*)	kg	845	845
Water (W)	kg	188	165
Superplasticizer (PRELOM® 300)	% by mass of C	1	3
W/C ratio	/	0.54	0.30
28 days compressive strength	MPa	37	61
28 days modulus of elasticity	GPa	36	40
28 days tensile strength	MPa	2.4	3.8

Table 1: mixes of the studied concretes B40 and B60.

2.2. Binders properties

The cement used in the B40 and B60 formula comes from the CALCIA Airvault factory in Western France (it is composed by 92 % of clinker and 6 % of limestone). Their main characteristics are presented in Table 2.

Physical characteristics	B40 and B60
Shrinkage at 28 days (µm/m)	720
Hardening (min)	225
Density (g/cm³)	3.13
Hydration heat (J/g)	(at 41 h) 315
Composition (%)	**B40 and B60**
Loss on ignition	3.35
SiO_2	**19.50**
Al_2O_3	3.35
Fe_2O_3	3.32
TiO_2	0.28
MnO	0.08
CaO	62.64
MgO	1.19
SO_3	2.73
K_2O	1.60
Na_2O	0.10
P_2O_5	0.52
S--	< 0.02
Cl-	0.03

Table 2: properties of the cement used for B40 and B60.

2.3. Aggregates properties

The B40 and B60 concretes have been fabricated with calcareous aggregates (99% $CaCO_3$) and siliceous sand (97% SiO_2). The granulometry curve (the same in both concretes) is given in Figure 1.

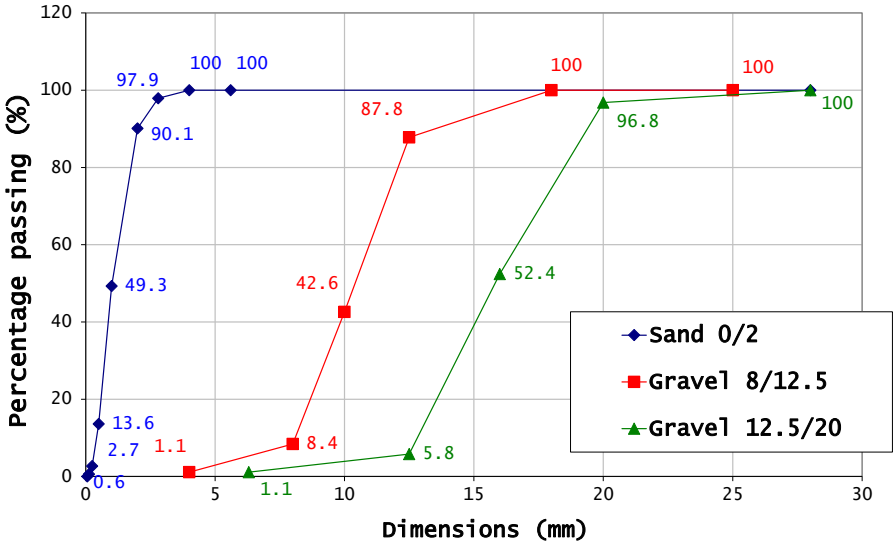

Figure 1: granulometry curve of B40 and B60 aggregates.

2.4. Storing conditions

For B40 and B60, the prismatic samples have been fabricated for pore pressure, temperature and mass measurements. Dimensions of the samples and experimental details are presented in separate sections. After casting, the samples are kept near the mixer (inner hall of the laboratory) in their moulds for 24 hours. The moulds are covered with plastic caps in order to avoid excessive evaporation of water. The samples are then removed from the moulds and placed in a 20 °C and a 50 % RH until the day of the test. A minimum of 90 days of conservation is respected before testing. The Table 3 gives the hydral state of the samples before tests.

	B40	B60
Days before test	154	126
Water content at the day of test (%)	2.59	3.46
Water porosity (%)	13.85	10.55
Bulk density (kg/m3)	2285	2364
Degree of saturation (%)	43	78

Table 3: hydral state of the samples before tests (mean values).

3. MAIN PROPERTIES OF CONCRETES VS TEMPERATURE

3.1. Water porosity

The concrete porosity was measured by a technique of water intrusion [1] and [12]. The operation of such a test is based on the recommendations of the AFREM [19] and is based on measuring the mass of a specimen of concrete (quarter-cylinder) in various states of saturation:

- Mass in the dry state m_{dry} : the mass of the specimen is measured after oven drying at 80 °C,
- Mass in the immersed saturated state m_{sat}^{imm} : the specimens are immersed in a bell vacuum (pressure of 25 mbar) for 24 hours. During this period, the porous network is assumed to be fully saturated with liquid water. The mass of the immersed specimen is then measured by hydrostatic weighing,
- Mass in the saturated state m_{sat} : the saturated specimen is taken out from the water and its mass is measured in the ambient air.

Water porosity of concrete (in %) is then calculated according to the expression (eq.1).

$$\Phi = \frac{m_{sat} - m_{dry}}{m_{sat\_} m_{sat}^{imm}} \times 100 \qquad \text{(eq.1)}$$

The water porosity of concrete is measured on specimens that have been thermally pre-treated at set temperature allowing to estimate the evolution of porosity with temperature. The heating rate and set values of temperatures for concretes are summarized in Table 4.

Before cooling and measurement of the porosity, the maximal temperature of the cycle is maintained during several hours in such a way that specimens are assumed to be in a homogeneous thermo-hygral state. The stabilization time must be long enough to ensure that most of the physico-chemical transformations and that the departure of water from the specimen are achieved. Hence, the stabilization time is longer at lower temperatures. The Table 5 presents the water porosity of B40 and B60 depending on the temperature. Figure 2 presents the evolution of the water porosity with temperature for B40 and B60. For concretes B40 and B60 the reference state corresponds to a dry material (obtained after drying for several days in an oven at 80 °C).

Concrete	Temperatures (°C)	Heating rate (°C/min)
B40 and B60	120, 250, 400	1.0

Table 4: heating rate and set values of temperatures for different concrete

Water porosity (%)		80 °C	120 °C	250 °C	400 °C
B40	**Test 1**	13.9	13.6	14.5	16.0
	Test 2	13.8	13.8	14.1	15.9
	Mean	13.85	13.0	14.30	15.95
B60	**Test 1**	10.2	11.3	12.8	13.9
	Test 2	10.9	11.7	13.5	14.2
	Mean	10.55	11.50	13.15	14.05

Table 5: water porosity after different thermal exposure (residual measurements) for B40 and B60

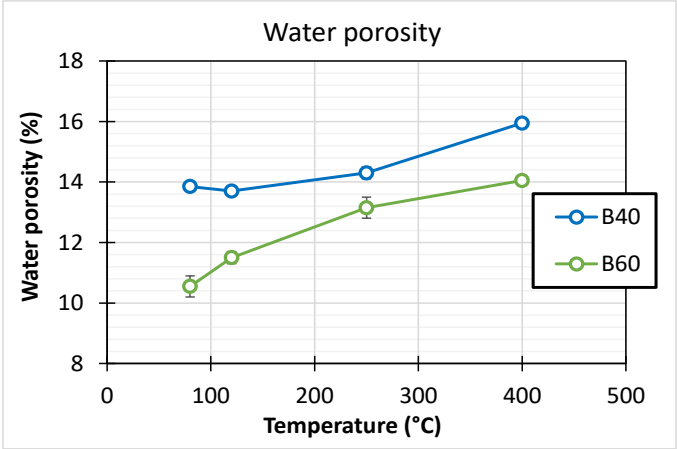

Figure 2: water porosity vs. temperature (mean values) for B40 and B60.

3.2. Density

The apparent density for B40 and B60 and their changes with temperature are measured [1] and [12]. The evolution of the density with temperature is given in Figure 3 and Table.6.

Density (kg/m³)		80 °C	120 °C	250 °C	400 °C
B40	Test 1	2280	2286	2278	2241
	Test 2	2289	2302	2295	2248
	Mean	2285	2294	2287	2245
B60	Test 1	2379	2333	2332	2306
	Test 2	2349	2344	2309	2300
	Mean	2364	2339	2321	2303

Table 6: density after different thermal exposure (residual measurements) for B40 and B60

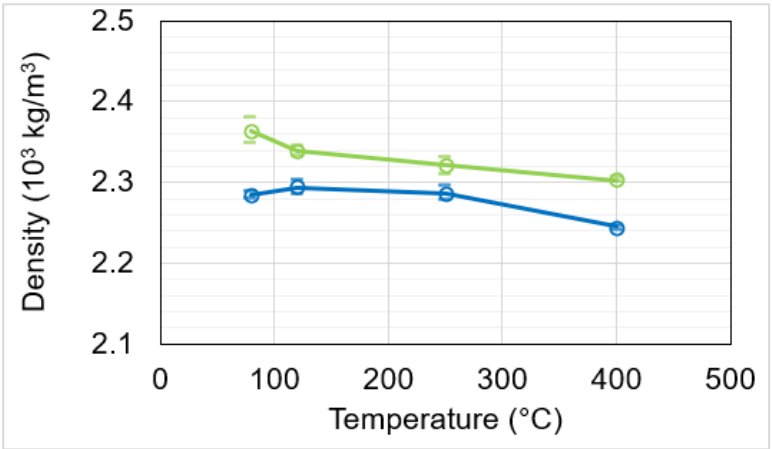

Figure 3: density vs. temperature (mean values) for B40 and B60.

3.3. Mass loss

Setup for experimental measurement of the loss of mass in transient heating was developed by Fire Technology division in SP Swedish laboratory, Figure 4 [1]. It consists of a cylindrical specimen (Ø104 mm, H50 mm) placed inside an electric furnace with circular radiating elements. During the test, the specimen is located in a perforated metal basket, suspended by an electronic balance. Balance is located on a rigid steel frame to minimize measurement noise caused by laboratory vibration and is connected to a computer during the test to measure continuous mass loss. Four thermocouples are located near the surface of the specimen. They are used for temperature records and additionally for the regulation of heating rate.

After measuring the initial mass, the specimen is exposed to heating rate of 1°C/min. The heating continues up to 600 °C. Figure 5 presents the changes in mass loss and mass loss rate with temperature for B40 and B60.

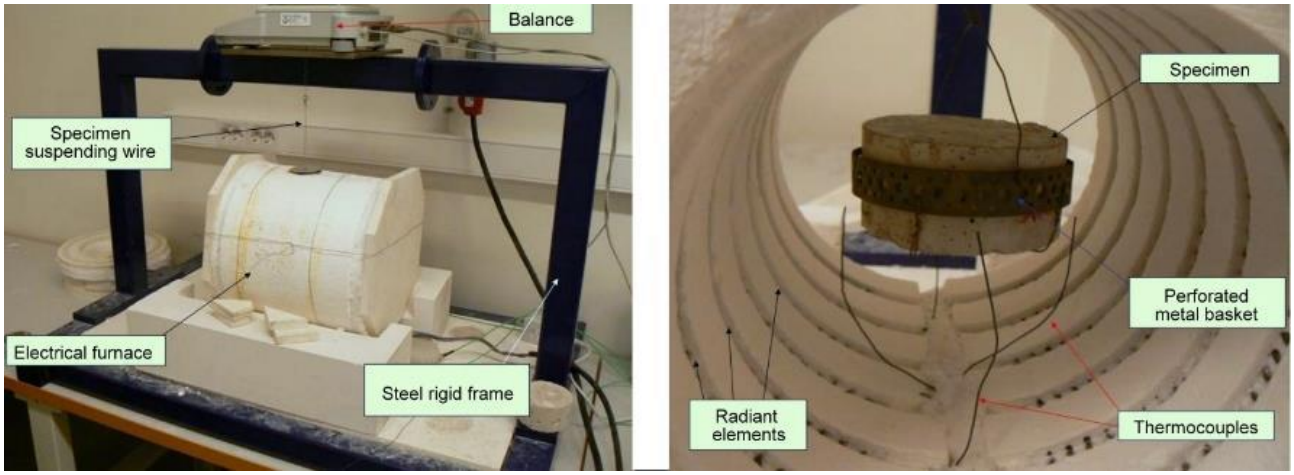

Figure 4: Setup for experimental measurement of the loss of mass in transient heating [1].

a)

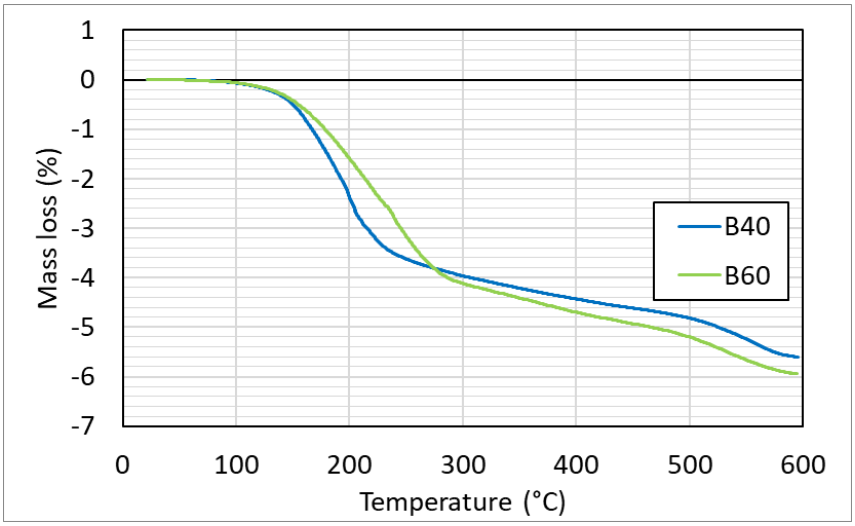

b)

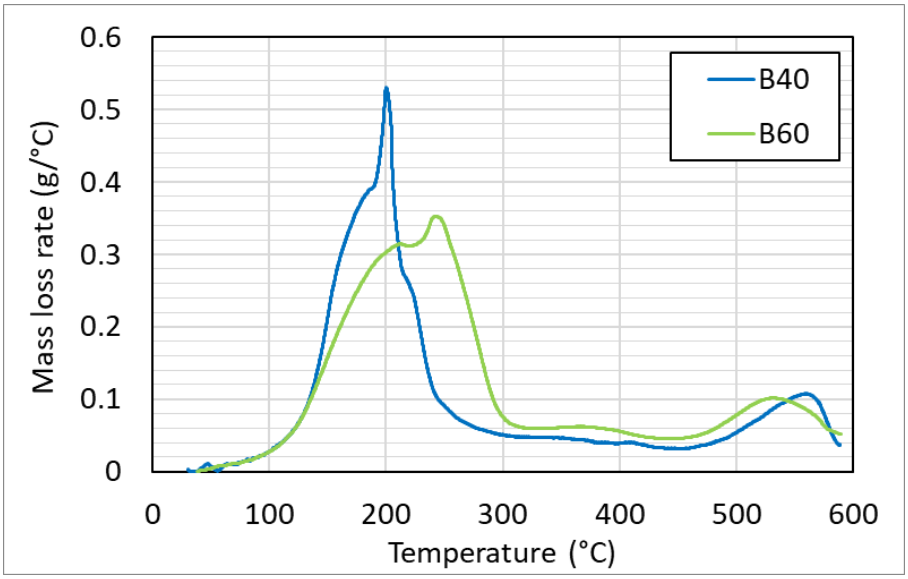

Figure 5: Results of: (a) mass loss and (b) mass loss rate vs. temperature for B40 and B60.

3.4. Gas permeability

The gas permeability of concrete is measured through a constant pressure permeameter (“CEMBUREAU” device) [1] and [12]. The procedure is based on the recommendations of the AFREM [19] and consists in measuring the gas flow (di-nitrogen) percolating through a concrete disk (150 mm in diameter and 50 mm thick). For each measure, two levels of gas pressure are applied in order to determine the intrinsic permeability of the material according to the Klinkenberg's approach [20].

The evolution of the concrete gas permeability with temperature is estimated by applying the same thermal cycles as for water porosity measurement (see § 3.1).

The concrete B40 and B60 are measured for temperature levels: 80 °C, 120 °C, 250 °C, 400 °C and 600 °C,

Table 7 presents the gas permeability of B40 and B60 depending on the temperature. Figure 6 presents the change of the gas permeability with temperature for B40 and B60.

Gas permeability (m^2)		80 °C	120 °C	250 °C	400 °C	600 °C
B40	Test 1	$5.0\ 10^{-16}$	$7.7\ 10^{-16}$	$1.2\ 10^{-15}$	$2.8\ 10^{-15}$	$1.8\ 10^{-13}$
	Test 2	$5.3\ 10^{-16}$	$5.5\ 10^{-16}$	$9.3\ 10^{-16}$	$5.7\ 10^{-15}$	$2.6\ 10^{-14}$
	Test 3	$6.28\ 10^{-16}$	$4.6\ 10^{-16}$	/	$4.1\ 10^{-15}$	$1.5\ 10^{-13}$
	Mean	$5.53\ 10^{-16}$	$5.93\ 10^{-16}$	$1.07\ 10^{-15}$	$4.2\ 10^{-15}$	$1.19\ 10^{-13}$
B60	Test 1	$2.1\ 10^{-16}$	$2.6\ 10^{-16}$	$4.9\ 10^{-16}$	$2.0\ 10^{-14}$	$2.8\ 10^{-14}$
	Test 2	$1.7\ 10^{-16}$	$1.2\ 10^{-16}$	**$5.91\ 10^{-16}$**	$2.2\ 10^{-14}$	$2.5\ 10^{-14}$
	Test 3	$1.2\ 10^{-16}$	$1.8\ 10^{-16}$	$2.9\ 10^{-16}$	$4.1\ 10^{-15}$	$1.7\ 10^{-14}$
	Mean	$1.67\ 10^{-16}$	$1.87\ 10^{-16}$	$4.57\ 10^{-16}$	$1.54\ 10^{-14}$	$2.33\ 10^{-14}$

Table 7: gas permeability after different thermal exposure (residual measurements) for B40 and B60.

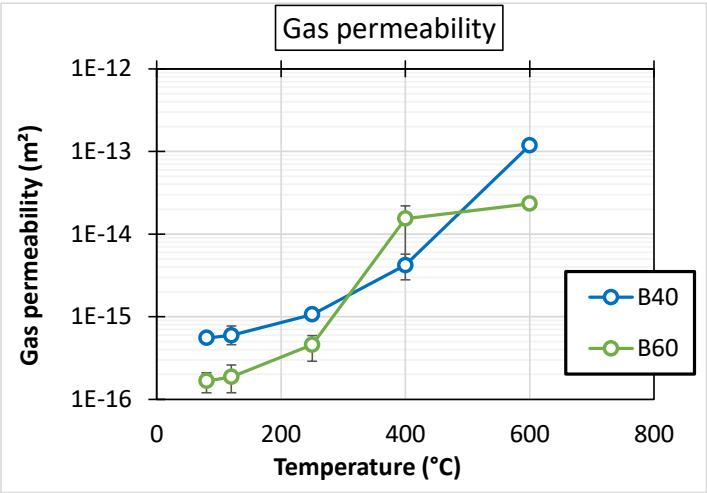

Figure 6: gas permeability vs. temperature (mean values) for B40 and B60.

3.5. Thermal properties at steady state

The thermal properties of concrete (thermal diffusivity and thermal conductivity) were measured at steady state by mean of the so-called "TPS" (Transient Plane Source) method, developed by [21]. Table 8 gives the thermal properties measured at ambient temperature for all materials. To estimate the change of the thermal conductivity with temperature, the specimens and the TPS resistivity sensor can be placed in an oven. Figure 7 presents this change for B40 and B60 concretes.

	Thermal conductivity (W/mK)	Specific Heat (J/kgK)	Density (kg/m^3)	Thermal diffusivity (mm^2/s)
B40	2.55	910	2285	1.23
B60	2.42	1020	2364	1.00

Table 8: thermal properties at 20 °C (TPS measurement).

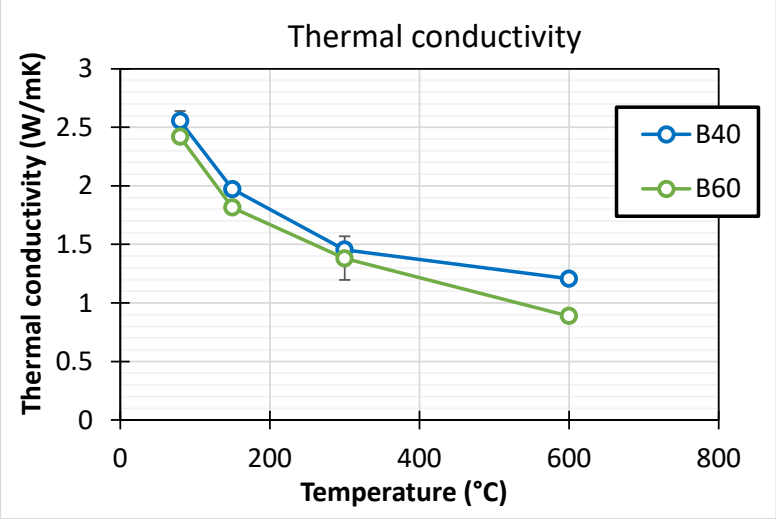

Figure 7: thermal conductivity vs. temperature (TPS measurement) for B40 and B 60.

3.6. Thermal expansion

The mechanical properties at high temperatures were measured on cylindrical specimens (diameter of 104 mm, 300 mm height) [1] and [6]. These specimens are placed in a cylindrical oven. A system for measuring strains in longitudinal direction of the specimen is coupled with the furnace. The entire device can be placed between the plates of a hydraulic press, which allows measurements of mechanical properties at high temperature. More details on the experimental device are presented in [1], [4], [6], [14], [22] and [23].

Samples (diameter 104 mm and height 300 mm) are heated at 1 °C/min until 600 °C. During the heating phase, different strains can be measured:

- **Free thermal strain (FS):** this is the strain of the sample in the longitudinal direction, without any mechanical loading

Figure 8 presents the thermal expansion of B40 and B60 measured until 600 °C with a heating rate of 1 °C/min.

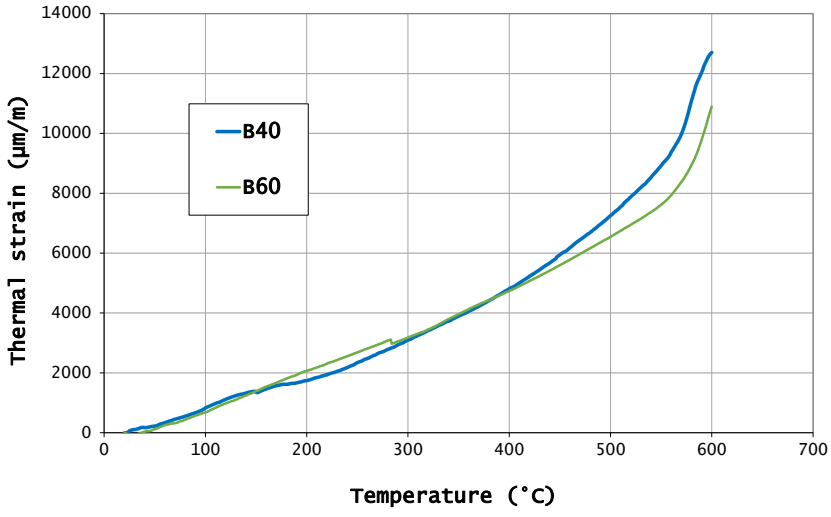

Figure 8: thermal expansion (heating rate: 1°C/min), B40 and B60.

3.7. Compressive strength and modulus of elasticity

The same device described in § 3.5 has been used for measuring the compressive strength and modulus of elasticity of concretes [1]. Tests have been performed at ambient temperature and then in hot conditions at 120, 250, 400 and 600 °C on samples (diameter 104 mm and height 300 mm). B60 has been tested only for 600 °C. The measured properties and their evolution with temperature are presented in Table 9 and Figure 9 for the compressive strength, and Table 10 and Figure 10 for the modulus of elasticity. The modulus of elasticity is defined as the slope of the stress / strain curve between the origin of the curve and the point corresponding to 30 % of the compressive strength of the material.

Compressive strength (MPa)	20 °C	120 °C	250 °C	400 °C	600 °C
B40	30	23	27	26	16
B60	67	/	/	/	27

Table 9: compressive strength (hot measurements, mean walues).

Modulus of elasticity (GPa)	20 °C	120 °C	250 °C	400 °C	600 °C
B40	24	14	13	8	3
B60	39	/	/	/	7

Table 10: modulus of elasticity (hot measurements, mean walues).

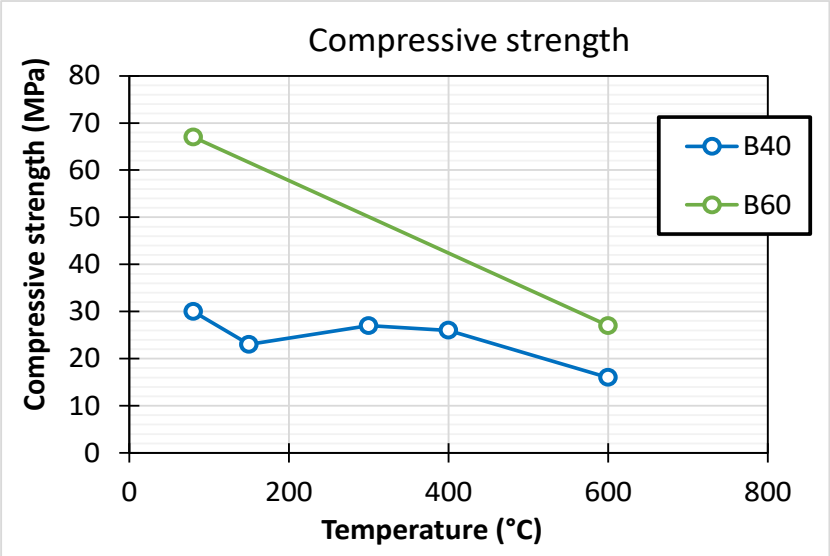

Figure 9: compressive strength vs. temperature for B40 and B60.

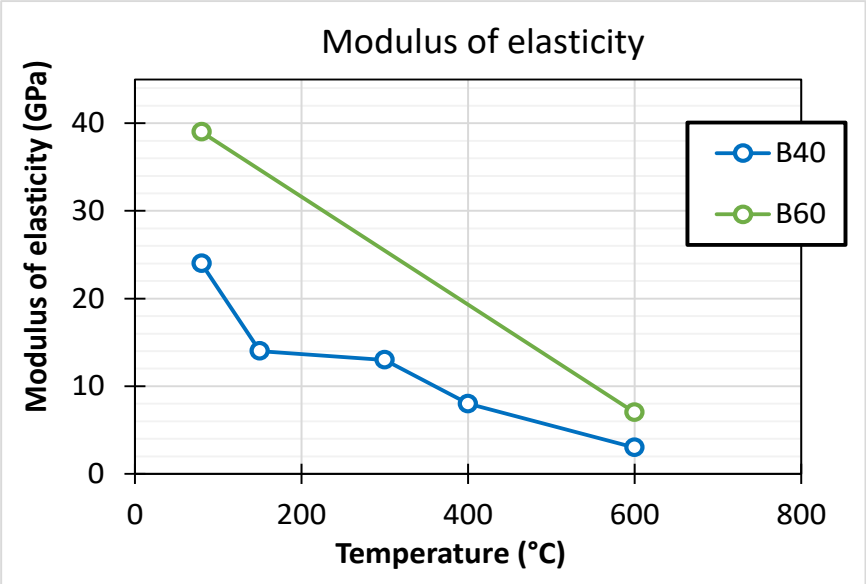

Figure 10: modulus of elasticity vs. temperature for B40 and B60.

3.8. Transient thermal strain

The same device described in § 3.5 has been used for determining the transient thermal stain of concretes [1] and [6].

Samples were heated with no load (free thermal strain presented in § 3.6) and under constant compressive stress corresponding to 20 % and 40 % of their ultimate strength a room temperature. Determined curves are presented in Figure 11.

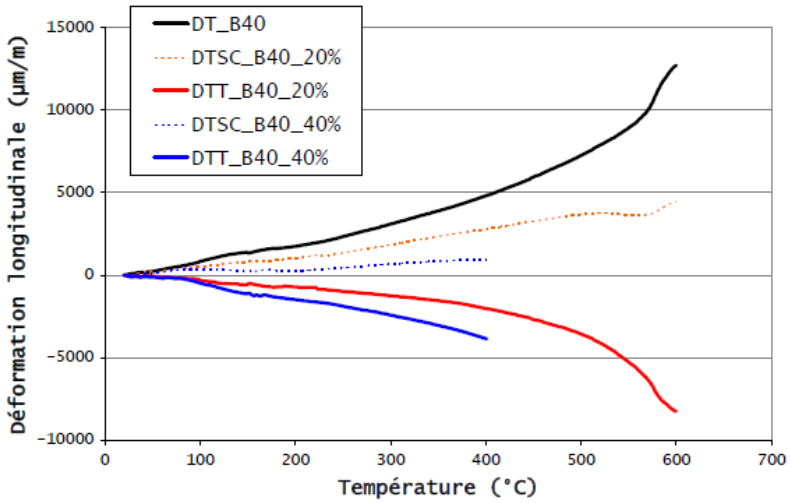

Figure 11: support for 3-points bending test.

3.9. Fracture energy and flexural strength

Fracture energy and flexural strength has been determined for B40 concrete [24]. Specimens were prisms of 10 x 10 x 35 cm. They were notched at mid-span up to the half of their height. This allows the localization of the cracks and the better control of the tests.

A test device shown in Figure 12 and Figure 13 was developed. It allows carrying out bending tests on specimens 10 cm x 10 cm x 35 cm. The distance between the two lower rollers is 30 cm. The test device was designed to carry out bending tests with isostatic load conditions.

The heating rate was 1 °C/min. The target temperature was maintained during 2 hours at 120 °C and 1 hour at the others temperatures (250 °C, 400 °C and 600 °C).

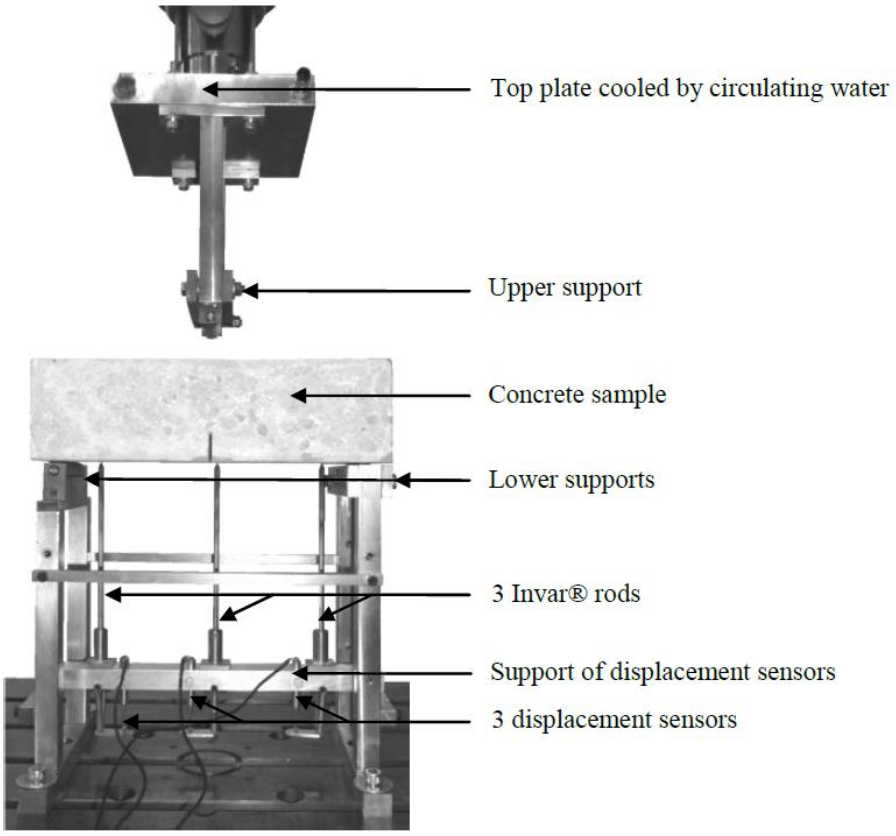

Figure 12: support for 3-points bending test.

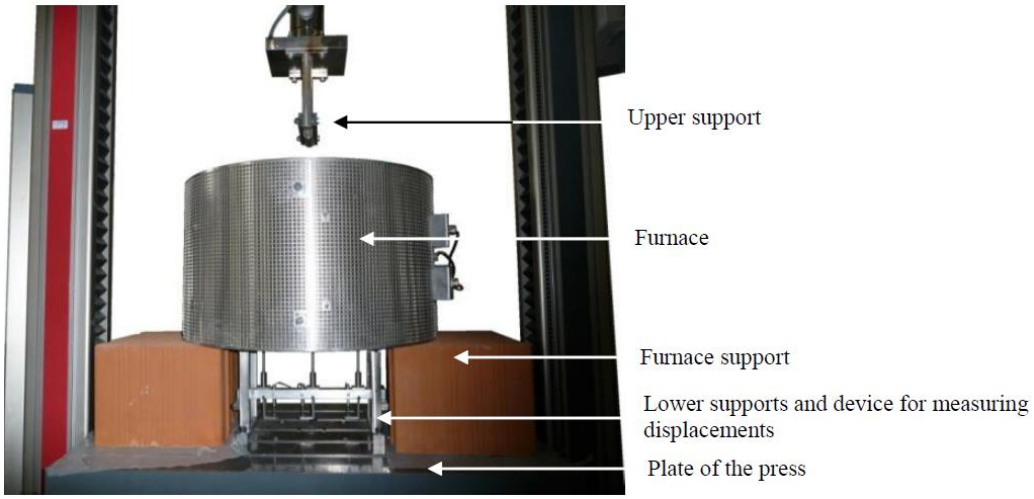

Figure 13: complete device test 3-point bending at high temperature.

The tests were carried out with an electromechanical press. Vertical displacements were measured in three points: at the edge of the notch (at mid-span) and at 3 cm from the supports. Vertical rods are made in Invar®. They pass through the furnace at the lower part. They are held in contact with the specimen by means of springs and guided by linear ball bearings. Three displacement sensors measure the displacement of the three rods relative to their support.

The details of the experimental setups are presented in [24].

In the elastic range, the relationship between the experimental measured displacement $\delta_{measured}$ and the true deflection (deflection at mid-span) can be calculated by using simple elastic based theories equations.

The experimental measured displacement $\delta_{measured}$ is defined as follows:

$$\delta_{measured} = \Delta_{mid\text{-}span} - (\Delta_1 + \Delta_2)/2$$

where:

$\Delta_{mid\text{-}span}$ is the measured displacement at mid-span,

Δ_1 and Δ_2 are the measured displacements near the 2 supports (the distance between the supports and the sensors is 3,5 cm).

Beyond the elastic range, deflection has been calculated by using the finite element code CAST3M.

Curves giving the strength as a function of $\delta_{measured}$ determined at different temperatures are plotted in Figure 13. Except at 120 °C, two samples were tested for each temperature. Obtained curves were smooth and regular. They were very close at each temperature. These 2 observations are satisfactory. In Figure 14, only one curve is plotted. One of the tests at 600 °C was unstable. Then, from the 2 tests carried out at this temperature, two values of maximum load and only one value of fracture energy (G_f) have been determined.

Figure 15 shows the curves of true deflection as a function of the applied load. The method presented in previous paragraph has been used to determine mid-span deflection from the measured displacement.

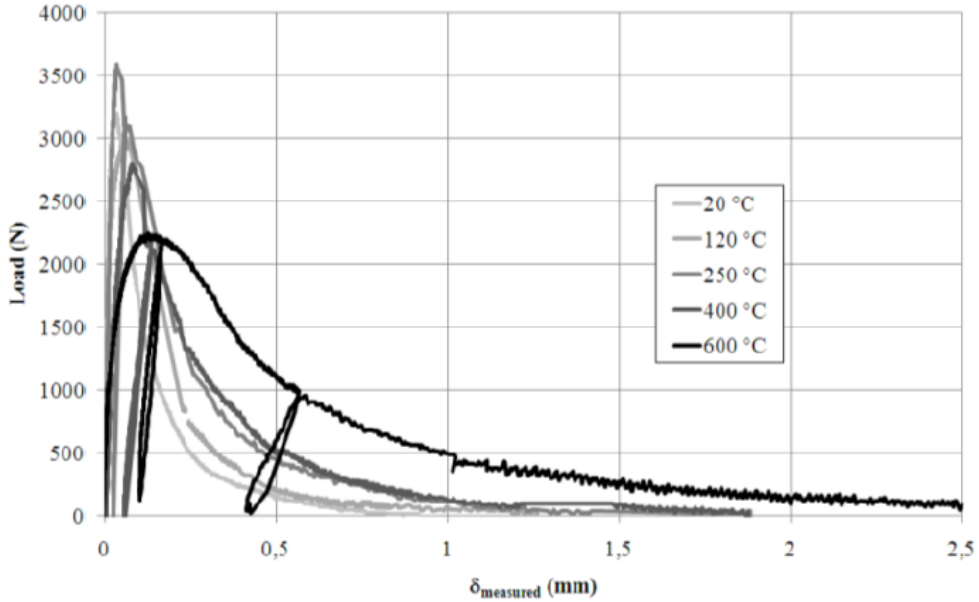

Figure 14: measured displacement as a function of the applied load

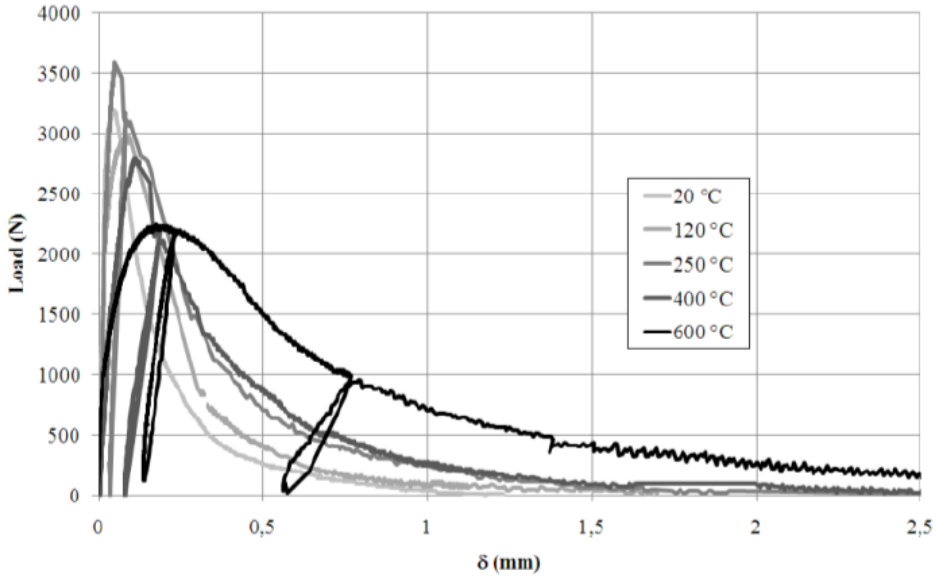

Figure 15: applied load versus mid-span deflection

v

The maximum load and the calculated fracture energy are given in Table 11.
Fracture energy was calculated according to the following equation:

$$G_f = \frac{W}{B(D - a_0)}$$

where W, B, D, a_0 are respectively the work supplied to statically fracture the notched specimen (area under the curve in Figure 16), specimen thickness, specimen height, notch length.

The maximum load and the flexural strength are quasi constant between 20 and 400 °C (Figure 16 and Figure 17). The values at 600 °C are lower. G_f increases from 20 °C to 600 °C (Figure 18). The values at 250 and 400 °C are very close.

B40		20 °C	120 °C	250 °C	400 °C	600 °C
Maximum load [N]	**Test 1**	3198	2979	2661	3333	2051
	Test 2	3186		3589	2795	2246
	Mean	**3192**	**2979**	**3125**	**3064**	**2148**
Fracture energy [J/m²]	**Test 1**	130	171	256	254	436
	Test 2			247	238	
	Mean	**130**	**171**	**252**	**246**	**436**
Flexural strength [MPa]	**Test 1**	5.8	5.4	4.8	6.0	3.7
	Test 2	5.7		6.5	5.0	4.0
	Mean	**5.7**	**5.4**	**5.6**	**5.5**	**3.9**

Table 11: fracture energy and flexural strength for B40 (hot measurements).

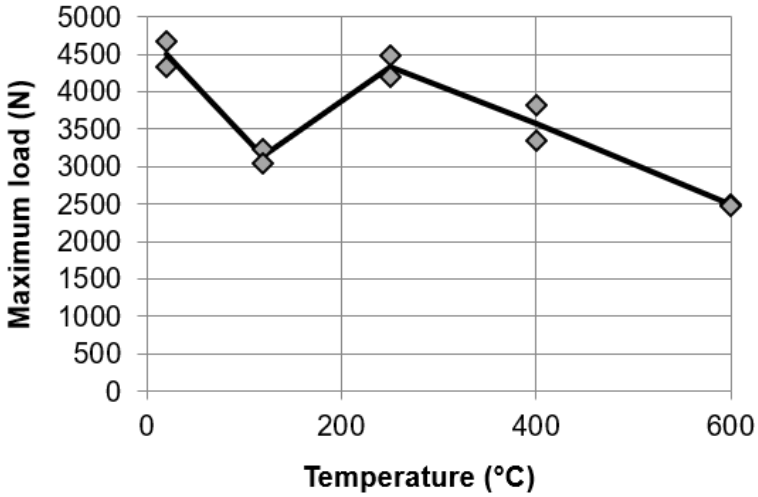

Figure 16: Maximum load in 3-point bending test versus temperature for B40

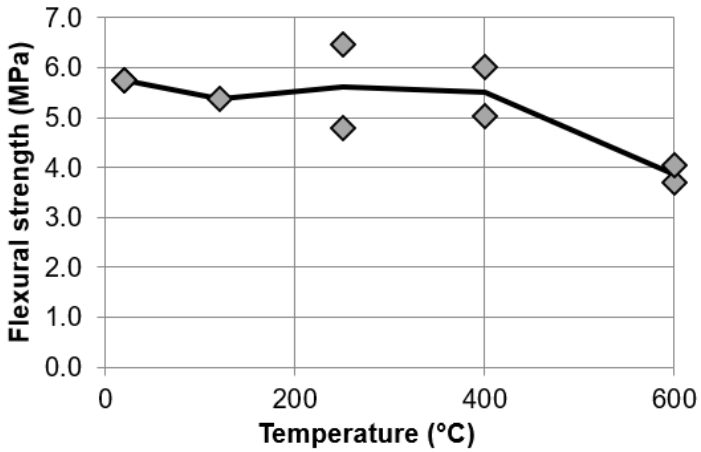

Figure 17: Flexural strengt versus temperature for B40

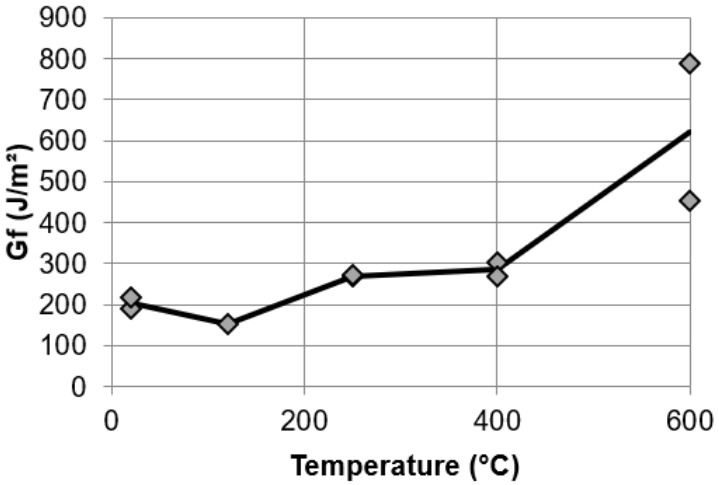

Figure 18: Fracture energy versus temperature for B40

3.10. Pore pressure, temperature and mass loss measurement

3.10.1. Experimental settings

The tests were carried out on prismatic samples (300 × 300 × 120 mm^3) heated on one side [1], [12] and [17]. The experimental device allows temperature and pore gas pressure to be measured in a concrete specimen during a transient heating (see Figure 19) [1], [25] and [26]. Before concrete casting, five metallic tubes (inner diameter of 1.6 mm) are placed in the molds. A sintered metal round plate (diameter 12 mm, thickness 1 mm) is wedded to the extremity of the tube that is placed into concrete. Just prior to tests, type K thermocouples (diameter 1.5 mm) are put in these tubes. It is worth noting that the free volume between the tube and the thermocouple (130 mm^3) were not filled with any sort of fluid, which can be different than other similar studies. The gas pressure in concrete is first transmitted via the metallic tubes to an external "T-junction", and then to an external pressure transducer (piezo-electrical transducer) via plastic tubes filled with silicon oil. By this way, temperature and pore gas pressure are simultaneously measured at the same location. Measurements are done at 2, 10, 20, 30, 40, and 50 mm from the heated surface. The thermal loading is ensured by a ceramic radiant panel (5 kW), covering the entire surface of the specimen and located 3 cm above it. The four sides of the concrete specimen are insulated by porous ceramic blocks. The heat flow can be then considered as unidimensional.

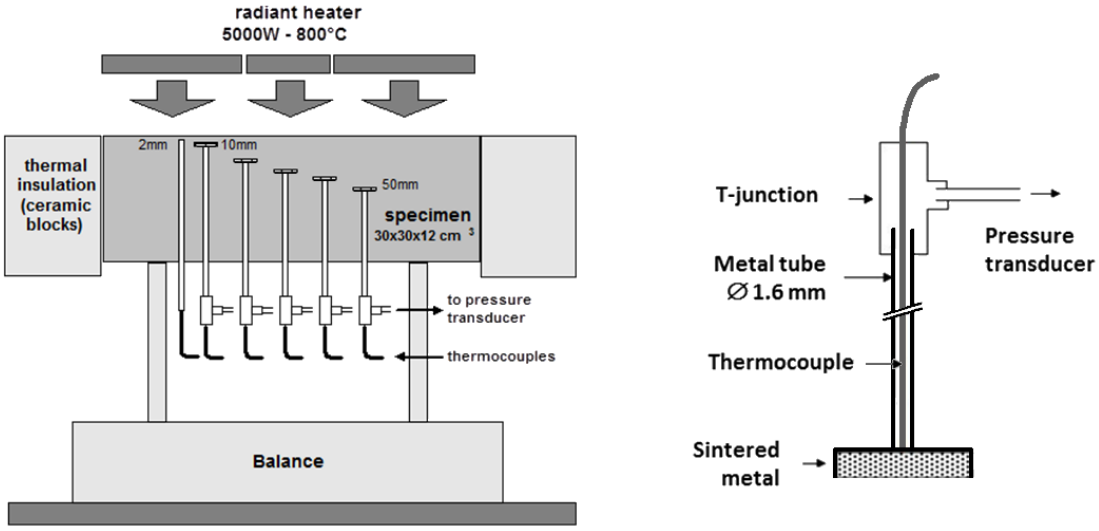

Figure 19: Scheme of the experimental set-up for small-scale tests (left). Right: detail of a metal tube filled with a thermocouple and connected to a "T-junction".

The effect of the thermal loading was studied for B40 and B60 in the following way. A reference thermal loading, called "**moderate heating**", is defined as following: the radiant panel is controlled in such a way that the temperature measured inside the panel reaches 600 °C as fast as possible (cf. Figure 20). The power of the panel is then kept constant in order to maintain this temperature of 600 °C during 5 hours. The sample is finally naturally cooled down. A second heating scenario, called "**high heating**", consists in controlling the radiant panel in such a way that its temperature reaches 800 °C as fast as possible (cf. Figure 20). Temperature is then maintained at 800 °C during 5 hours, after which the sample naturally cools down. Other tests are carried out on the B40 with a thermal scenario called "**slow heating**": temperature in the radiant panel gradually increases up to 600 °C, with a heating rate of 10 °C/min. Temperature is then maintained at 600 °C during at least 5 hours, after which the sample naturally cools down. Figure 20 shows the evolution of

the temperature that is measured: i) inside the radiant panel, ii) in the sample (B40) at 10 mm from the exposed surface for the different scenario.

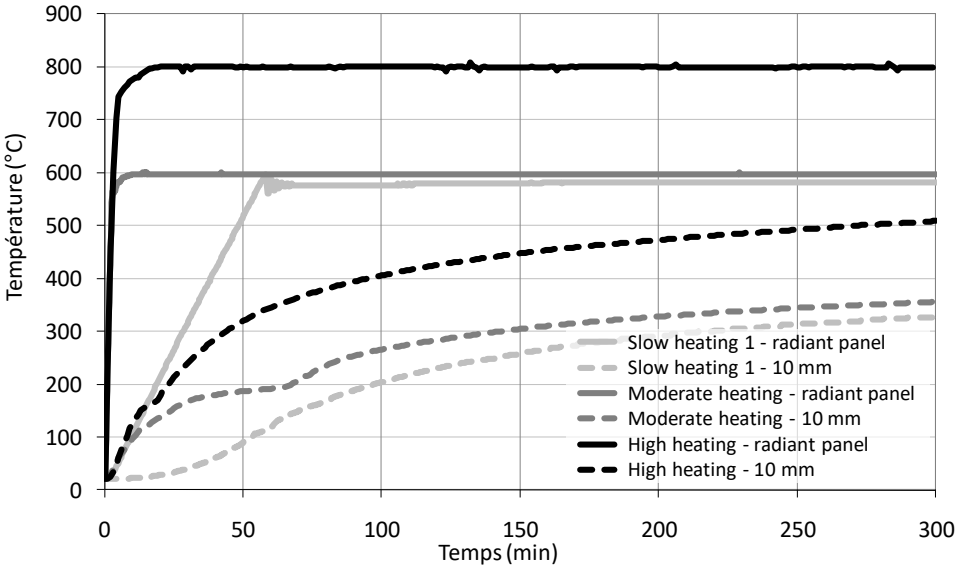

Figure 20: evolution of the temperature measured in the radiant panel and in the concrete (at 10 mm from the exposed surface) for the different thermal scenario.

NOTE: The PTM tests were also carried out for B40 and B60 concretes under the ISO834 fire exposure. The evolution of vapour pore pressure under ISO fire is presented in [9].

3.10.2. Results

For B40 and B60 concretes, two tests have been done for the “high” and “moderate” heating. Only one test has been done for the “slow” heating” on the B40, none on the B60.

The time evolution of the temperature, the pore gas pressure and the mass loss of each sample are presented in the next pages.

3.10.2.1. Temperature measurement

➢ **Temperature of B40**

Tinf = unexsposed side

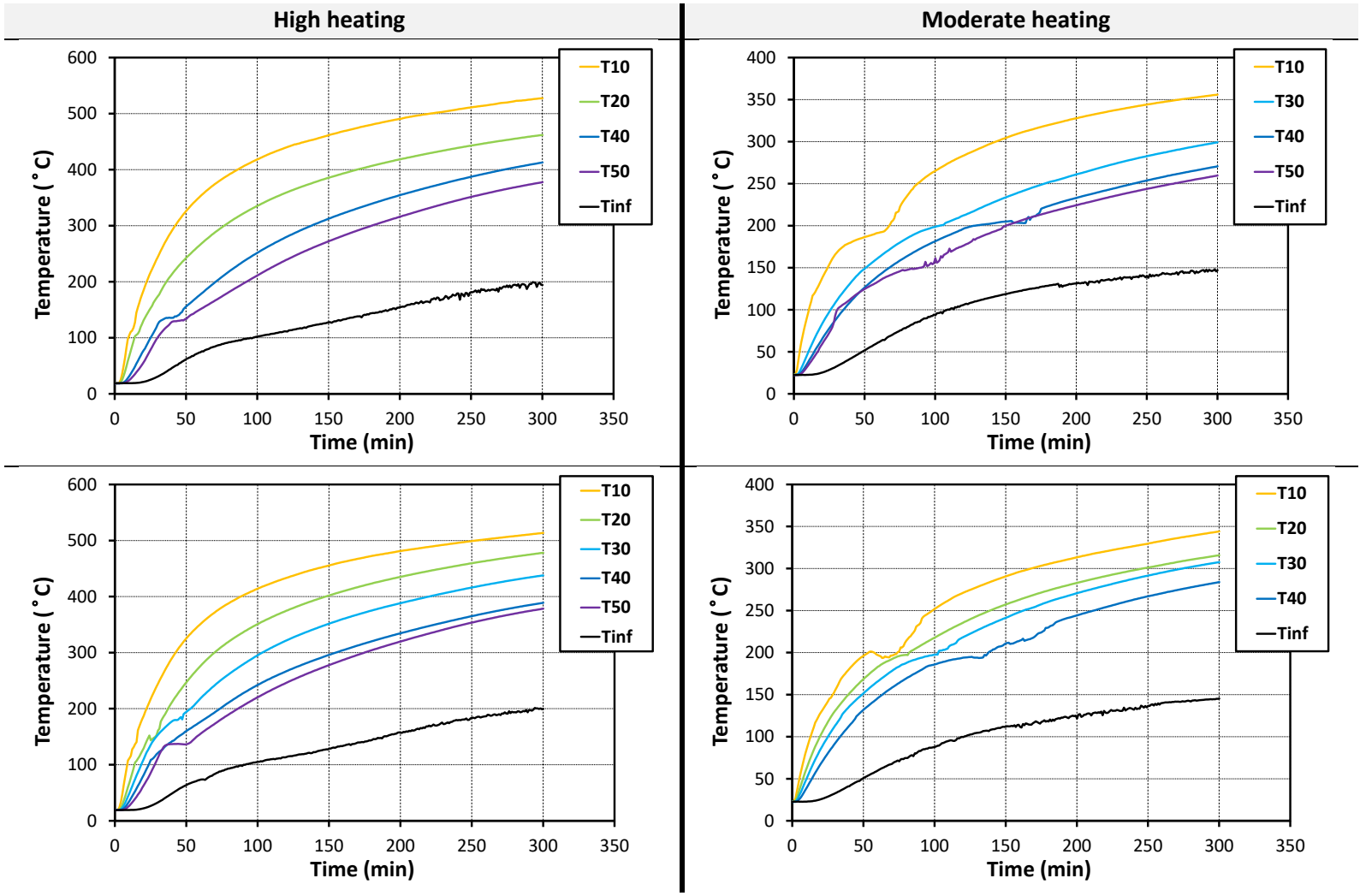

Slow heating 10°C/min	Slow heating 1°C/min
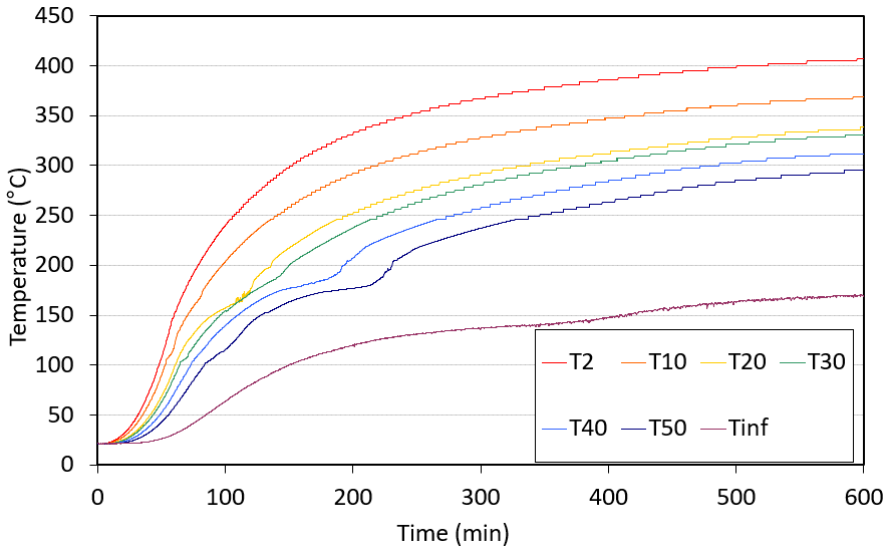	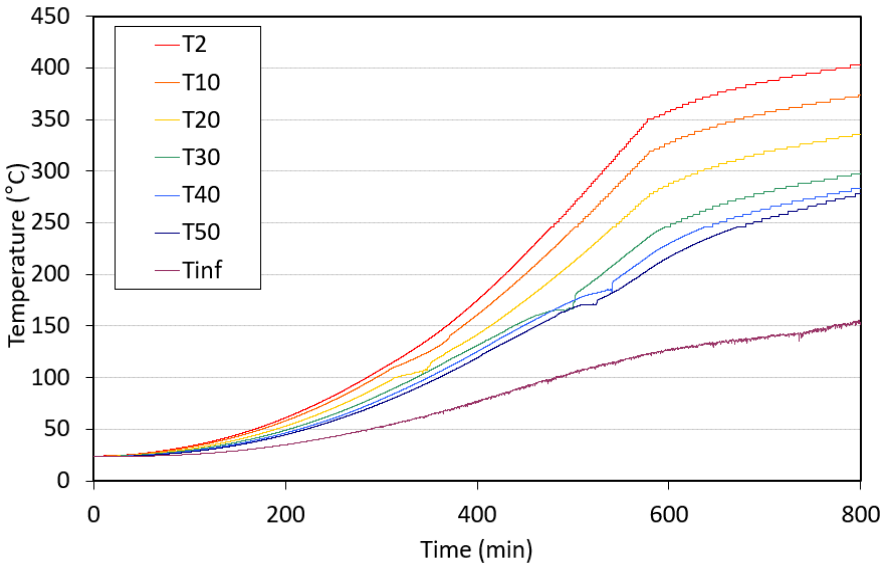

➢ **Temperature of B60**

Tinf = unexsposed side

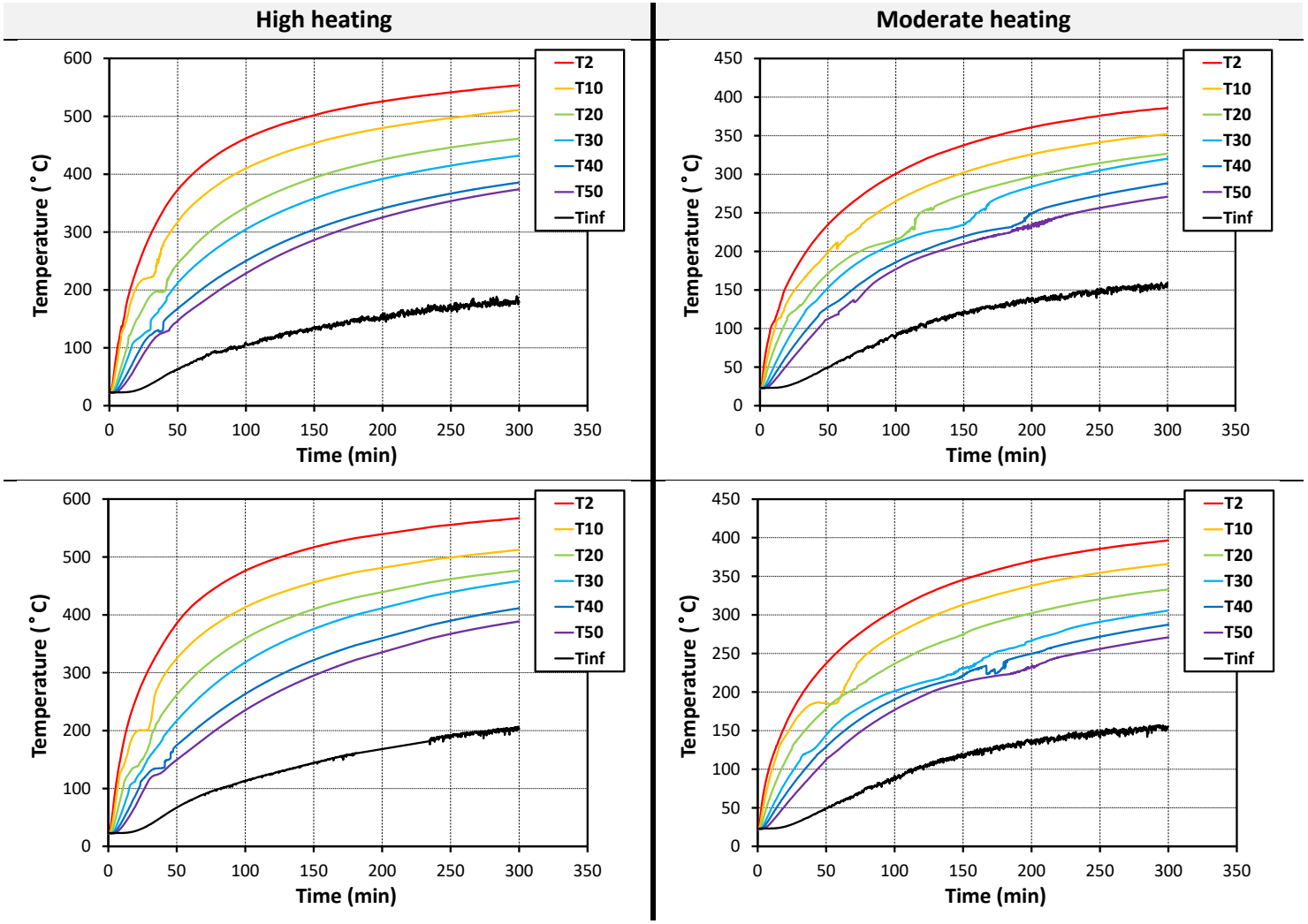

3.10.2.1. Pressure measurement

➢ **Pore gas pressure of B40**

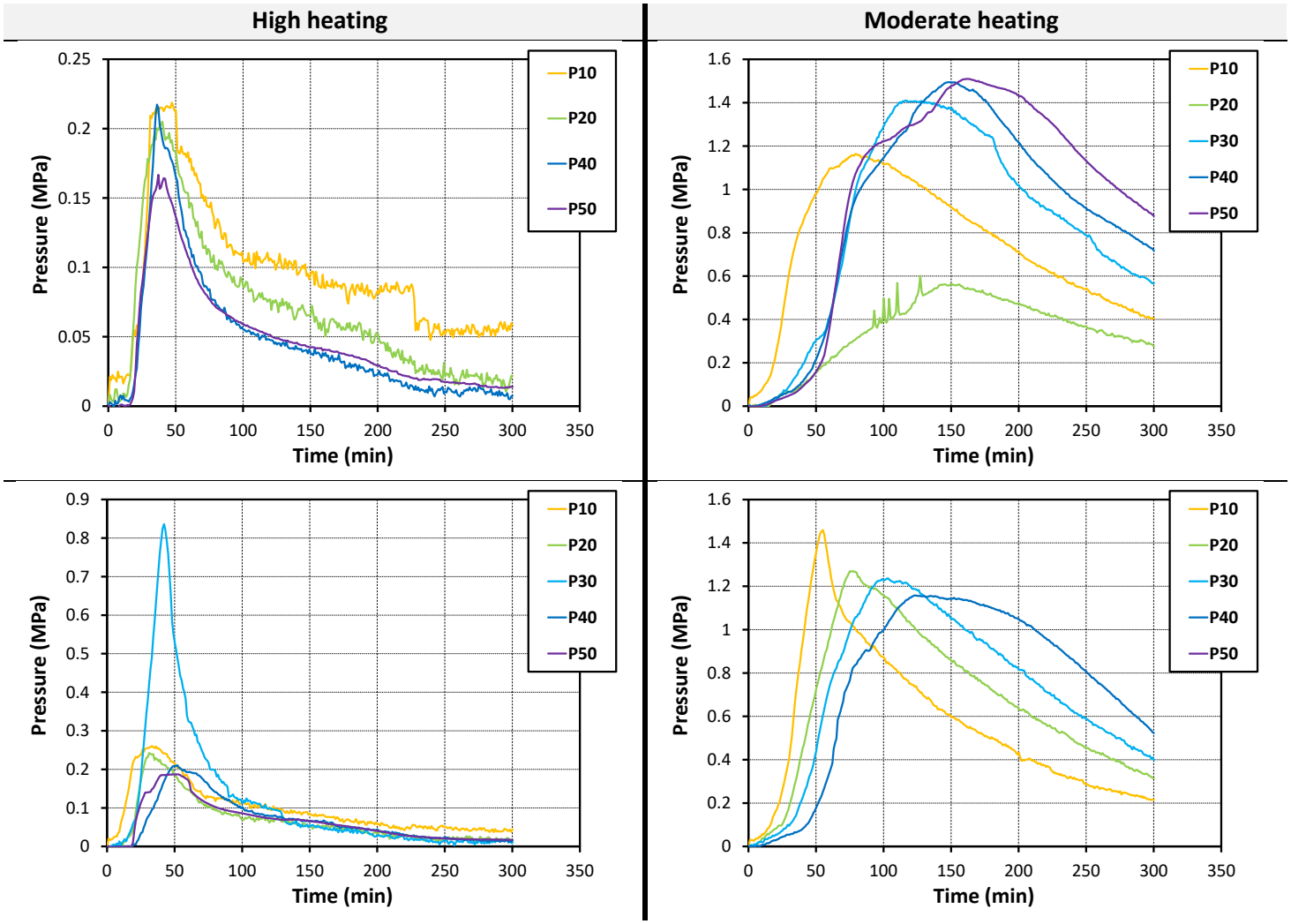

Slow heating 10°C/min	Slow heating 1°C/min
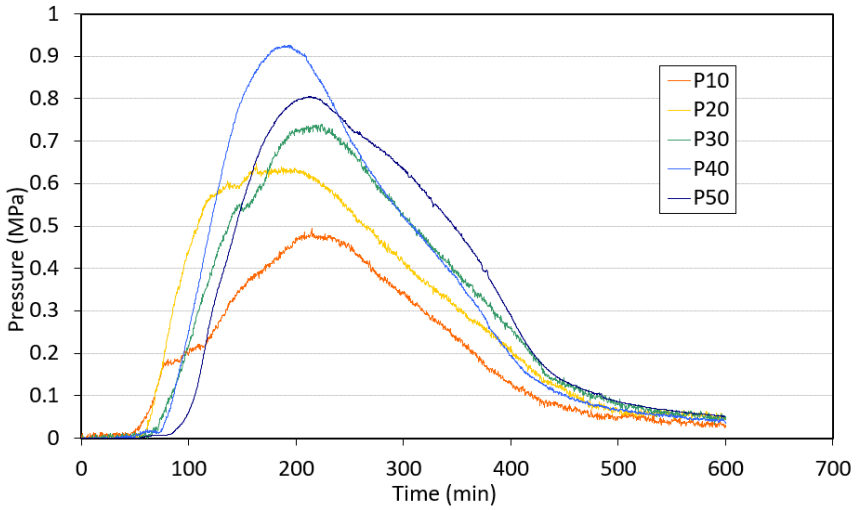	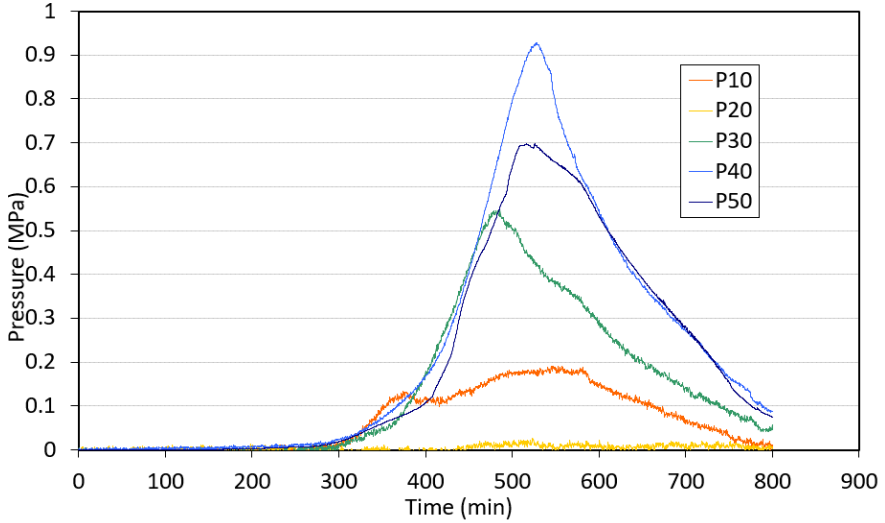

➢ **Pore gas pressure of B60**

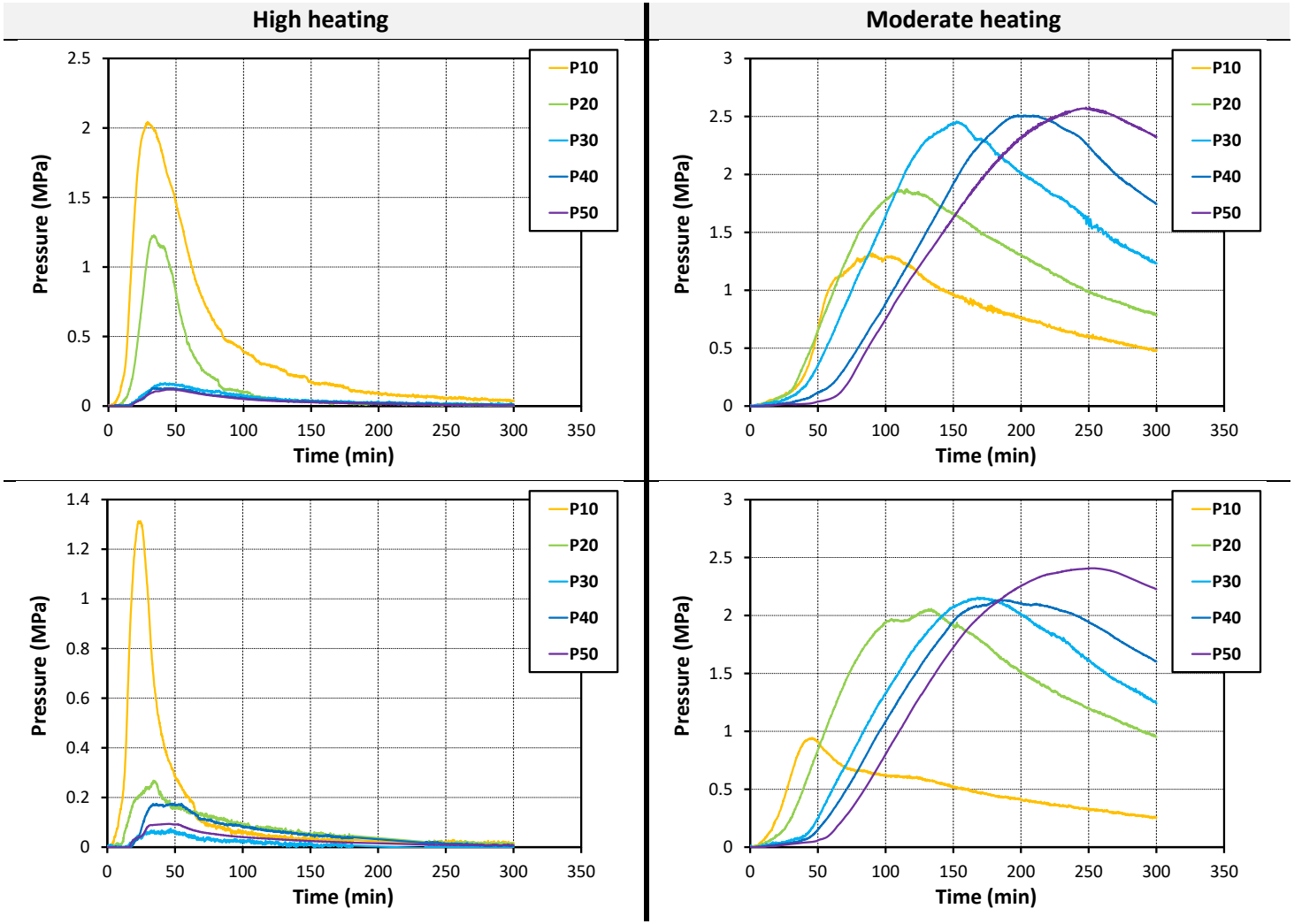

3.10.2.1. Mass measurement

➢ **Mass loss of B40**

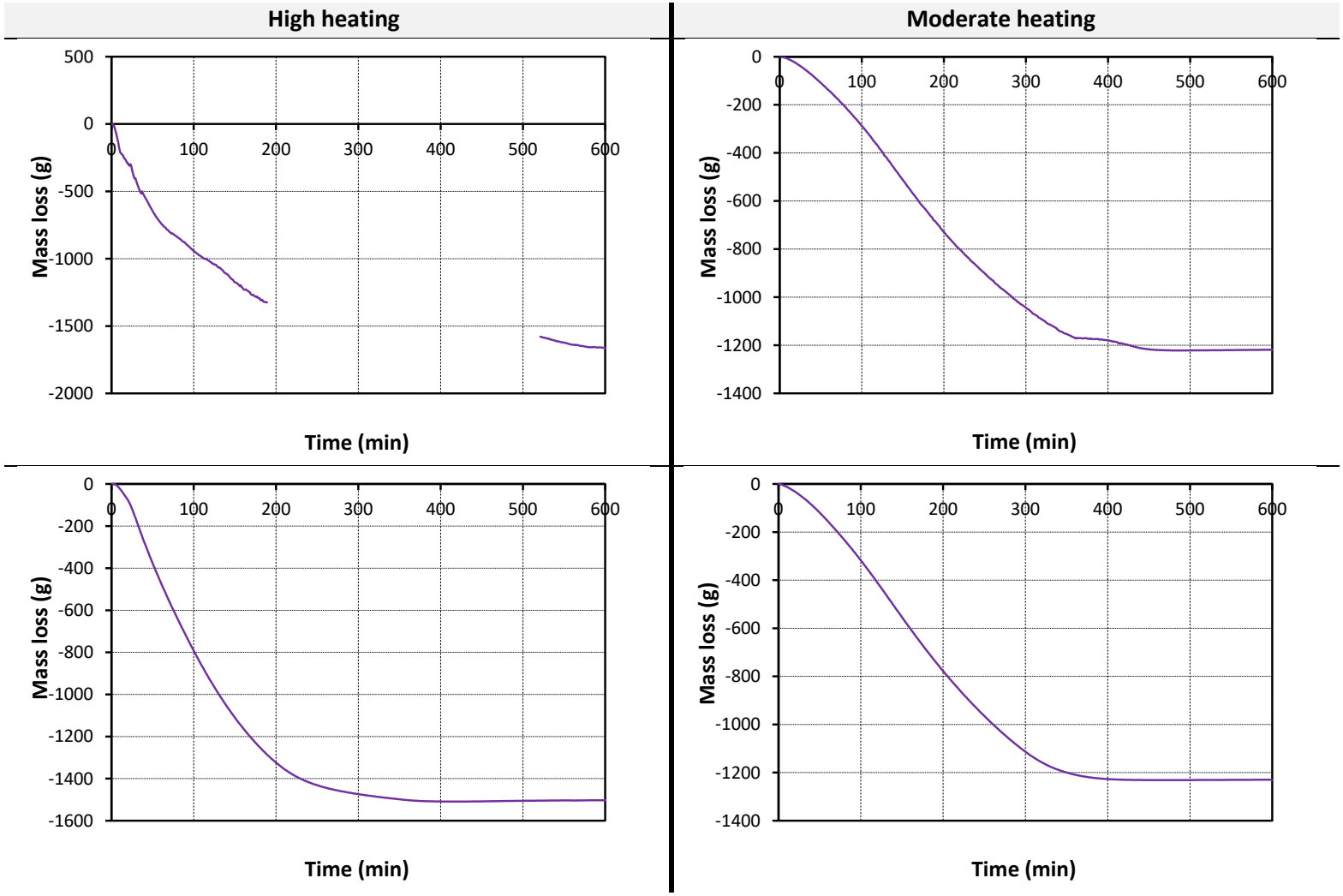

Slow heating 10°C/min	Slow heating 1°C/min
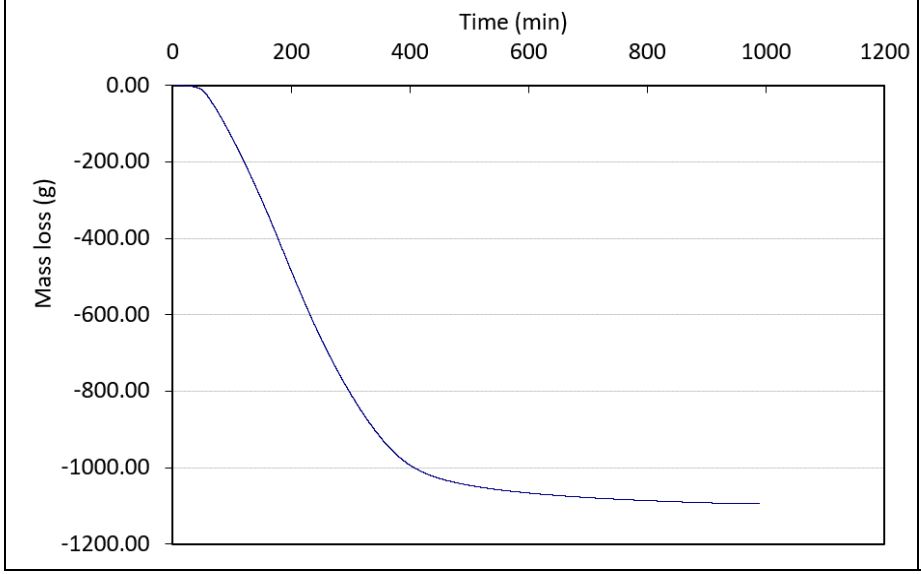	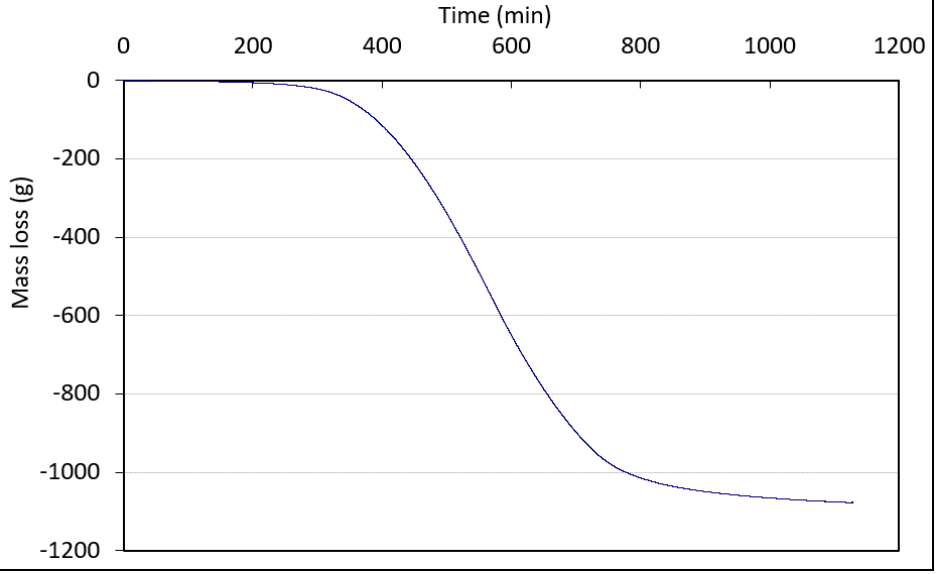

➢ **Mass loss of B60**

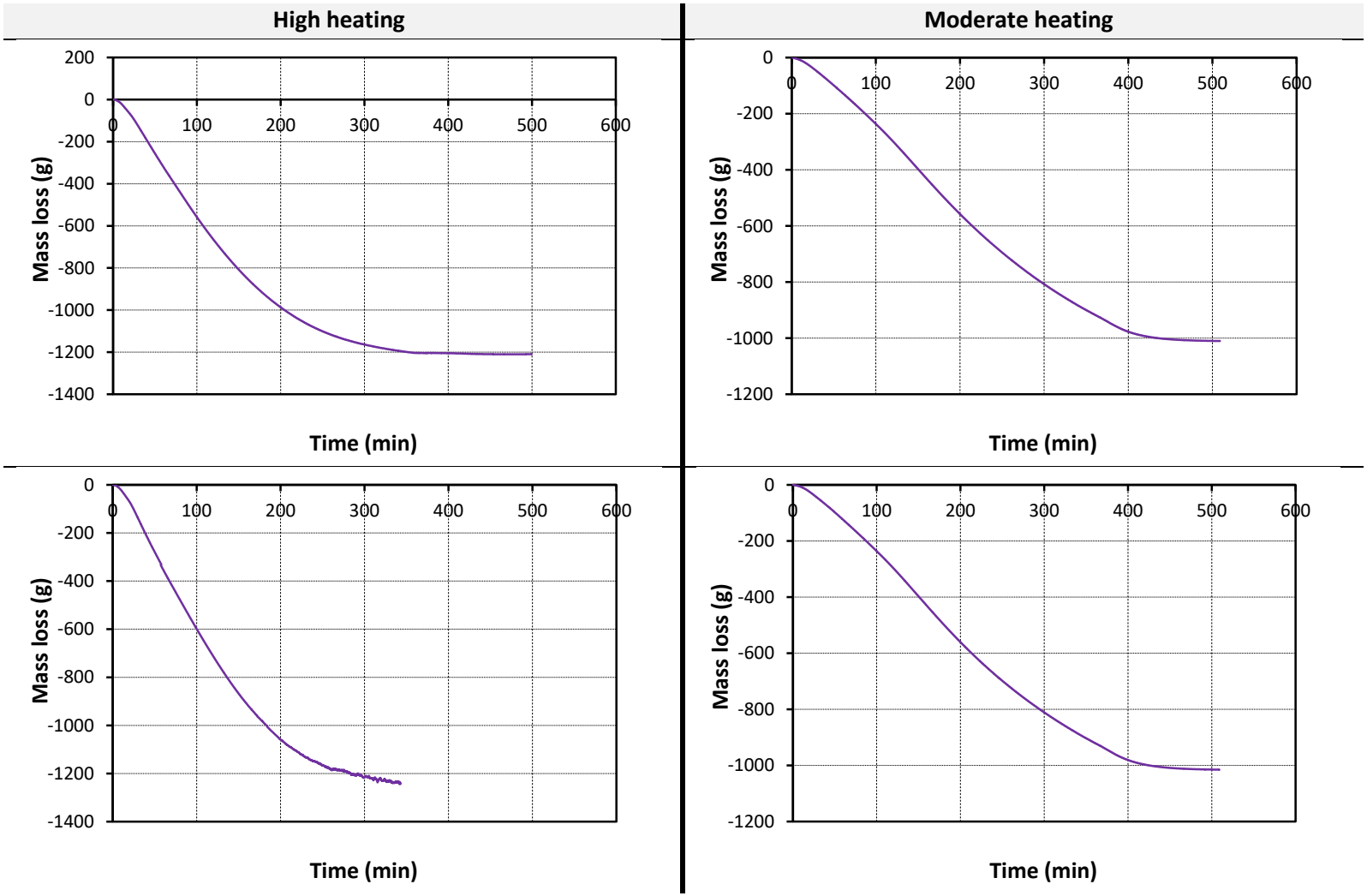

4. OTHER PROPERTIES OF B40 AND B60 CONCRETES

We have reported on section 3 the main properties (mass transport, thermal, mechanical) which have been studied on concrete B40 and B60. We have also reported results from the test PTM (Pressure, Temperature and Mass).

In this section 4, we give the references of the publications on a large number of tests have also been carried out on fire exposed intermediate-scale and large-scale specimens made from these 2 concretes.

Mass transport	
Tests on intrinsic permeability under different confining pressures	[27], [28], [29]
Combined NMR moisture, temperature and pressure measurements on small cylinder exposed to heating	[30]
Mechanical properties	
Moisture effect on mechanical behavior of concrete at high temperature	[31]
Thermo-mechanical behaviour on large scale tests	
Thermo Mechanical Experimental Investigation on 3 Loaded Concrete Walls Exposed to ISO 834-1 Fire	[32] [33]
Pore pressure	
Tests on pore vapour pressure measurements on cylinders, prisms and slabs exposed to different fire scenarios (slow, moderate, rapid and ISO 834-1)	[9]
Tests on pore vapour pressure measurements and fire spalling on slabs exposed to ISO 834-1 and HC_{inc} fire scenarios	[17]
PTM (pore, pressure, Temperature and Mass) on small slabs – Influence of cement type (CEM II and CEM III)	[34], [35]
Fire spalling mechanism	
Influence of pore pressure on fracture behaviour of concrete during heating. Combined splitting test and pore pressure measurement	[36], [37]
Combined use of Acoustic Emission (AE) and pore Pressure and Temperature (PT) measurements on slabs exposed to ISO 834-1 and HCinc fire scenarios	[38]
Fire spalling mechanism tests on intermediate-scale slabs	
Effect of Biaxial Mechanical Loading and Cement Type on the Fire Spalling Behaviour of Concrete", P	[39], [40], [41], [42], [43]
Fire spalling mechanism tests on large-scale slabs	
Fire spalling tests on large slabs exposed to ISO 834-1 and HCinc fire scenarios under unloaded and loaded conditions	[44],[45], [46]
A comparative study on spalling behaviour of embedded cores and slabs exposed to HCinc fire scenario	[47]

5. LITERATURE REFERENCES

[1] Mindeguia J.C., “Contribution expérimentale à la compréhension des risques d'instabilité thermique des bétons”, PhD thesis of the Université of Pau and Pays de l'Adour, July 2009. *In French.*

[2] Jean-Christophe MINDEGUIA, Pierre PIMIENTA, Izabela HAGER, Christian LA BORDERIE, Hélène CARRÉ, "Experimental study of transient thermal strain and creep of an ordinary concrete at high temperatures", Fourth International Workshop on Structures in Fire SIF'06, Aveiro, Portugal, 10-12 May 2006.

[3] Jean-Christophe MINDEGUIA, Hélène CARRÉ, Pierre PIMIENTA, Christian LA BORDERIE, "Nouvelle technique de mesure des déformations transversales du béton à hautes températures", 24èmes Rencontres Universitaires de Génie Civil, La Grande Motte, France, 01-02 Juin 2006.

[4] MINDEGUIA J.C., CARRÉ H., PIMIENTA P., LA BORDERIE Ch. CSTB Département Sécurité, Structures et Feu, Université de Pau et des Pays de l'Adour. A new experimental device for assessing the radial strains of concrete at high temperatures, Revue Européenne de Génie Civil. Volume 11. N° 9-10/2007. p 1187-1198.

[5] MINDEGUIA J.C., PIMIENTA P., LA BORDERIE Ch., CARRÉ H. CSTB Département Sécurité, Structures et Feu, Université de Pau et des Pays de l'Adour. Experimental study of mechanical behaviour of high performance concretes at high temperature, Fib Workshop "FIRE DESIGN OF CONCRETE STRUCTURES - FROM MATERIALS MODELLING TO STRUCTURAL PERFORMANCE", Coimbra, Portugal, 8-9 November 2007.

[6] MINDEGUIA J.C., PIMIENTA P., BEUROTTE A., LA BORDERIE Ch., CARRÉ H.. CSTB Département Sécurité, Structures et Feu, Université de Pau et des Pays de l'Adour. Experimental study of fire behaviour of different concretes – Thermo-hydral and spalling analysis, Fib Workshop "FIRE DESIGN OF CONCRETE STRUCTURES - FROM MATERIALS MODELLING TO STRUCTURAL PERFORMANCE", Coimbra, Portugal, 8-9 November 2007.

[7] CARRE H., MINDEGUIA J.C., LA BORDERIE Ch., PIMIENTA P. CSTB Département Sécurité, Structures et Feu, Université de Pau et des Pays de l'Adour. Dispositif d'Observation de la microstructure et de pesée des bétons au cours d'un chauffage. Annales du Bâtiment et des Travaux Publics. N°5. Octobre 2007. 8 pages. Article présenté au 25èmes Rencontres Universitaires du Génie Civil, Bordeaux, France, 23 – 25 Mai 2007.

[8] JEAN-CHRISTOPHE MINDEGUIA, PIERRE PIMIENTA, HELENE CARRE, CHRISTIAN LABORDERIE. Contribution expérimentale à la compréhension des risques d'instabilité thermique des bétons. Influence de la nature des granulats. Colloque AUGC 2009, 27èmes Rencontres Universitaires de Génie Civil. Saint Malo. Mai 2009.

[9] Mindeguia, J.-Ch., Pimienta, P., Carré, H., La Borderie, Ch. “Experimental study on the contribution of pore vapour pressure to the thermal instability risk of concrete”. 1st international workshop on concrete spalling due to fire exposure, Leipzig, Germany. 150-167, 2009.

[10] JEAN-CHRISTOPHE MINDEGUIA, PIERRE PIMIENTA, ALBERT NOUMOWE, MULUMBA KANEMA Temperature, pore pressure and mass variation of concrete subjected to high temperature – Experimental and numerical discussion on spalling risk. Cement and Concrete Research, Volume 40, Issue 3, March 2010, Pages 477-487.

[11] MINDEGUIA JEAN-CHRISTOPHE, PIMIENTA PIERRE, HAGER IZABELA, CARRÉ HÉLÈNE. Influence of water content on gas pore pressure in concretes at high temperature. 2nd International RILEM Workshop on Concrete Spalling due to Fire Exposure. 5-7 October 2011, Delft, The Netherlands, pp 113-121.

[12] MINDEGUIA J.C., PIMIENTA P., CARRE H., LA BORDERIE C. On the influence of aggregate nature on concrete behaviour at high temperature. European Journal of Environmental and Civil Engineering, 16/2, February 2012, p. 236-253 [doi:10.1080/19648189.2012.667682]

[13] MINDEGUIA J.C., CARRE H., LA BORDERIE C., PIMIENTA P. Analyse expérimentale du risque d'instabilité thermique des bétons en situation d'incendie. AUGC-IBPSA 2012, XXXe Rencontres universitaires de génie civil 'constructions durables' : recueil des communications, présentations. Tome 1, 6-8 juin 2012, Chambéry, FRA, 11 p.

[14] MINDEGUIA J.C./HAGER I./PIMIENTA P./CARRE H./LA BORDERIE C. Parametrical study of transient thermal strain of ordinary and high performance concrete. Cement and Concrete Research, 48, June 2013, p. 40-52 [doi:10.1016/j.cemconres.2013.02.004]

[15] MINDEGUIA J.C./PIMIENTA P./CARRE H./LA BORDERIE C. Experimental analysis of concrete spalling due to fire exposure. European Journal of Environmental and Civil Engineering, Published online: 17 Apr 2013, April 2013, 14 p. [doi:10.1080/19648189.2013.786245]

[16] H. Carré, P. Pimienta, C. La Borderie, F. Pereira and J.-C. Mindeguia. Effect of compressive loading on the risk of spalling. 3rd International RILEM Workshop on Concrete Spalling due to Fire Exposure. 25-27 September 2013, Paris, France, MATEC Web of Conferences, Vol. 6 (2013)

[17] MINDEGUIA J.C., CARRE H., PIMIENTA P., LA BORDERIE C. Experimental discussion on the mechanisms behind the fire spalling of concrete. Fire & Materials, Article first published online, June 2014, 17 p. [doi:10.1002/fam.2254]

[18] Mindeguia J.C., Carré H., Pimienta P., La Borderie C., “Experimental discussion on the mechanisms behind the fire spalling of concrete”, Fire And Materials, Vol. 39, no 7, pp. 619-635, 2015.

[19] AFREM, “Compte rendu des journées techniques AFPC-AFREM – Durabilité des bétons. Laboratoire Matériaux de Durabilité des Constructions”, INSA Toulouse, December 1997. *In French.*

[20] Klinkenberg L.J., "The permeability of porous media to liquid and gases." Drilling and Production Practice, 200-231, 1941.

[21] Gustafsson S.E., Long, T., "Transient Plane Source (TPS) for Measuring Thermal Properties of Building Materials." Fire and Materials, n°19: 43-49., 1995.

[22] Hager, I., 2004. Comportement à haute température des bétons à haute performance - évolution des principales propriétés mécaniques (in French) (PhD Thesis). Ecole Nationale des Ponts et Chaussées.

[23] Hager, I., Pimienta, P., 2005. Transient thermal strains of High Performance Concretes. Presented at the Concreep7, International conference on creep, shrinkage and durability of concrete and concrete structures, Nantes, France, p. 12.

[24] Carré, H., Pimienta, P. “Bending test at high temperature”. 15th International Conference on Experimental Mechanics, ICEM15, Porto, Paper 3802, 2012.

[25] Kalifa, P., F.D. Menneteau and Quénard D. (2000). "Spalling and Pore Pressure in HPC at high temperatures. Cement and Concrete Research 30 1915-1927.

[26] Kalifa, P., G. Chéné, et al. (2001). "High-temperature behaviour of HPC with polypropylene fibres: From spalling to microstructure." Cement and Concrete Research 31(10): 1487-1499.

[27] Carré, H., Céline, P., Atef, D., Miah, M. J., and Bassem, A. (2016). “Durability of Ordinary Concrete after Heating at High Temperature”, The 8th International Conference on Concrete under Severe Conditions-Environment and Loading, September 12-14, 2016, Politecnico di Milano, Lecco, Italy

[28] MIAH J.M./KALLEL H./CARRE H./PIMIENTA P./PINOTEAU N./LA BORDERIE C./LO MONTE F./FELICETTI R. The effect of loading on the residual gas permeability of concrete
Concrete spalling due to fire exposure: 5th international workshop, Borås, SWE, October 12-13, 2017, Rise, SP Report, 2017:43:00, 2018 (=DOC00014912)

[29] Miah M J, Kallel H, Carré H, Pimienta P. La Borderie C The effect of compressive loading on the residual gas permeability of concrete, May 2019, Construction and Building Materials 217:12-19

[30] Pel L., Jaspers S., Pereira F. Pimienta P. and Carré H.. Combined NMR moisture, temperature and pressure measurements during heating. 3rd International RILEM Workshop on Concrete Spalling due to Fire Exposure. 25-27 September 2013, Paris, France, MATEC Web of Conferences, Vol. 6 (2013)

[31] Katarzyna KRZEMIEŃ-MROZ, Pierre PIMIENTA, Nicolas PINOTEAU. Moisture effect on mechanical behavior of concrete at high temperature and its implication on fire spalling. 4th international workshop, October 8-9, 2015, Leipzig, DEU, 10 p.

[32] Miah, M. J., Pinoteau N., and Pimienta, P. (2016). “A Thermo Mechanical Experimental Investigation on 3 Loaded Concrete Walls Exposed to ISO 834-1 Fire”, Proceedings of the 9th International Conference on Structures in Fire, June 8-10, 2016, Princeton, USA.

[33] Bamonte, P., Felicetti, R., Kalaba, N., Lo Monte, F., Pinoteau, N, Miah, M. J and Pimienta, P. “On the Structural Behavior of Reinforced Concrete Walls Exposed to Fire”, The 8th International Conference on Concrete under Severe Conditions-Environment and Loading, September 12-14, 2016, Politecnico di Milano, Lecco, Italy

[34] MIAH J.M., PIMIENTA P., CARRE H., PINOTEAU N., LA BORDERIE C. Effect of cement type on pore pressure, temperature and mass loss of concrete heated up to 800 ° AUGC 2015, 33e Rencontres universitaires de génie civil, "De la terre à la mer", 27-29 mai 2015, Bayonne, FRA, Université de Pau et des pays de l'Adour, 2015, p. 432-439

[35] MIAH J.M., PIMIENTA P., CARRE H., PINOTEAU N., LA BORDERIE C. Fire spalling of concrete: effect of cement type Concrete spalling due to fire exposure: 4th international workshop, October 8-9, 2015, Leipzig, DEU, 10 p.

[36] FELICETTI R., LO MONTE F., PIMIENTA P. The influence of pore pressure on the apparent tensile strength of concrete. SIF'2012, Structures in fire, Proceedings of the 7th International conference, June 6-8, 2012, Zürich, CHE, Empa/ETH Zürich, 2012, p. 589-598

[37] FELICETTI R./LO MONTE F./PIMIENTA P. A new test method to study the influence of pore pressure on fracture behaviour of concrete during heating. Cement and Concrete Research, 94 [doi:10.1016/j.cemconres.2017.01.002], April 2017 (=DOC00014434)

[38] F. Pereira, K. Pistol, M. Korzen, F. Weise, P. Pimienta, H. Carré, S. Huismann. Monitoring of fire damage processes in concrete by pore pressure and acoustic emission measurements. 2nd International RILEM Workshop on Concrete Spalling due to Fire Exposure. 5-7 October 2011, Delft, The Netherlands, pp 69-77

[39] Miah, M. J., Carré, H., Pimienta, P., Pinoteau, N., and La Borderie, C. (2015). “Effect of Uniaxial Mechanical Loading on Fire Spalling of Concrete,” Proceedings of 4th International Workshop on Concrete Spalling (IWCS) due to Fire Exposure, October 8-9, 2015, Leipzig, Germany.

[40] Miah, M. J., Lo Monte, F., Pimienta, P., and Felicetti, R. (2016). “Effect of Biaxial Mechanical Loading and Cement Type on the Fire Spalling Behaviour of Concrete”, Proceedings of the 9th International Conference on Structures in Fire, June 8-10, 2016, Princeton, USA.

[41] Miah, M. J., Lo Monte, F., Felicetti, R., Carré, H., Pimienta, P and La Borderie, C. (2016). “Fire Spalling Behaviour of Concrete: Role of Mechanical Loading (Uniaxial and Biaxial) and Cement Type”, The 8th International Conference on Concrete under Severe Conditions-Environment and Loading, September 12-14, 2016, Politecnico di Milano, Lecco, Italy

[42] MIAH J.M./LO MONTE F./FELICETTI R./PIMIENTA P./CARRE H./LA BORDERIE C.

Experimental investigation on fire spalling behaviour of concrete: effect of biaxial compressive loading and cement type

Concrete spalling due to fire exposure: 5th international workshop, Borås, SWE, October 12-13, 2017, Rise, SP Report, 2017:43:00, 2018 (=DOC00014910)

[43] MIAH MJ, LO MONTE F, FELICETTI R, PIMIENTA P, CARRÉ H, LA BORDERIE C. Impact of external biaxial compressive loading on the fire spalling behavior of normal-strength concrete. Construction and Building Materails. 366 (2023)

[44] Nicolas Taillefer, Cyril Quentin, Romuald Avenel. Spalling of concrete: a synthesis of experimental results for middle and large size tests. 1st International Workshop on Concrete Spalling due to Fire Exposure, Leipzig, Germany, 3-5 September 2009.

[45] Pimienta Pierre, Octavian Anton, Jean-Christophe Mindeguia, Romuald Avenel, Heidi Cuypers, Eric Cesmat. Fire protection of concrete structures exposed to fast fires. 4th International symposium on Tunnel Safety and Security (ISTSS), Frankfurt, Germany, 17th-18th March 2010.

[46] Pimienta Pierre, Octavian Anton, Jean-Christophe Mindeguia, Romuald Avenel, Heidi Cuypers, Eric Cesmat. Protection incendie des structures en beton exposees a des feux a combustion rapide. Publication de recherche Promat. 2011

[47] Pimienta P. Moreau B., Avenel R., Peyrac P., Taillefer N., Larive C., D’Aloia L. and Clec’h P. Spalling tests on embedded cores and slabs: A comparative study 3rd International RILEM Workshop on Concrete